2023 IEEE/ASME International Conference on Advanced Intelligent Mechatronics (AIM)
June 28-30, 2023. Seattle, Washington, USA

A Fully 3D Printed, Multi-Material, and High Operating Temperature Electromagnetic Actuator

Sebastian Mettes[1,*], Justin Bates[1], Kenneth W. Allen[2], and Yi C. Mazumdar[1]

***Abstract*— Three-dimensional (3D) printing concepts that combine electrically conductive and electrically insulating materials opens up new opportunities for the design and manufacturing of electromagnetic actuators. While significant research has been conducted to 3D print antennas and planar circuits using silver nanoparticle inks, little focus has been given towards high power (>1 W) actuator applications. In this work, we design a novel 3D printed, centimeter-scale, multi-layer electromagnetic actuator consisting of syringe deposited silver nanoparticle ink on layers of copper-particle-filled polylactic acid (PLA) polymer filament. The Cu-PLA material is not only electrically insulating at moderately high temperatures but is also higher density and more thermally conductive than traditional polymer filaments. These features enable higher operating temperatures, higher burst forces, and longer sustained output. To demonstrate this concept, we first outline the design, material selection, and 3D printing process for a 16-layer, single trace electromagnetic coil. Then, models for the thermal characteristics, force distribution, and mechanical response are developed and compared with experimental results. Measurements show that the electromagnetic coil can produce up to 46 mN of force over 4 mm of stroke with 6.3 W of input power, and can operate indefinitely with 4.2 W of input power at 140°C without external cooling. Several applications are demonstrated including a small compliant joint gripper and a speaker. Finally, a fully-integrated, multi-material, single-print actuator and gripper combination is demonstrated to illustrate how this work can be used to create fully-operational single-print mechatronic and robotic systems.**

I. INTRODUCTION

Multi-material additive manufacturing and three-dimensional (3D) printing enable new levels of customization for electromechanical devices [1] as well as opportunities for fast prototyping and integrated components. Recently, advances in multi-material 3D printing techniques, particularly with metallic nanoparticle inks [2], [3], have led to development of numerous small static transducers enabling embedded sensing of pressure [4], temperature [5] and strain [6]. Electrical components such as capacitors, inductors [7], and flexible circuit boards [8] have also been demonstrated. Silver nanoparticle inks have also been used to print micro-scale electromechanical 2D electrostatic-drive motors [9]. While these motors enable new design concepts, they are limited by their small scale and low force output.

In order to enable additively manufactured centimeter-scale robotic actuation, various methods for 3D printing electromagnetic coils and actuators have been investigated in the literature, including 5-axis 3D printing and automated winding of wire around printed cores [10], [11], the use of silver pastes [7], [12] to wrap 3D printed cores, and filling stereolithographically manufactured (SLA) channels with conductive liquid gallium alloys [13], [14], [15], [16], [17]. While wire winding is capable of achieving higher power actuation, the technique is limited to geometries that allow external application of copper wires over a 3D printed core. Fully additively manufactured electromagnetic coils, on the other hand, have more design flexibility but have only been able to achieve low output power levels (<1 A). In order to improve the state-of-the-art for 3D printed actuators, we recently demonstrated the design of centimeter-scale electromagnetic coil actuators manufactured using fused filament fabrication (FFF) with nGen [18] polymer filament and silver nanoparticle (AgNP) ink [19]. While these actuators were able to successfully achieve higher output levels, the electrically and thermally insulating 3D-printed plastic substrates deflected at 70°C, severely limiting operating times, actuator lifetimes, heat transfer capabilities, steady state output power levels, and applications. To make fully 3D printed actuators

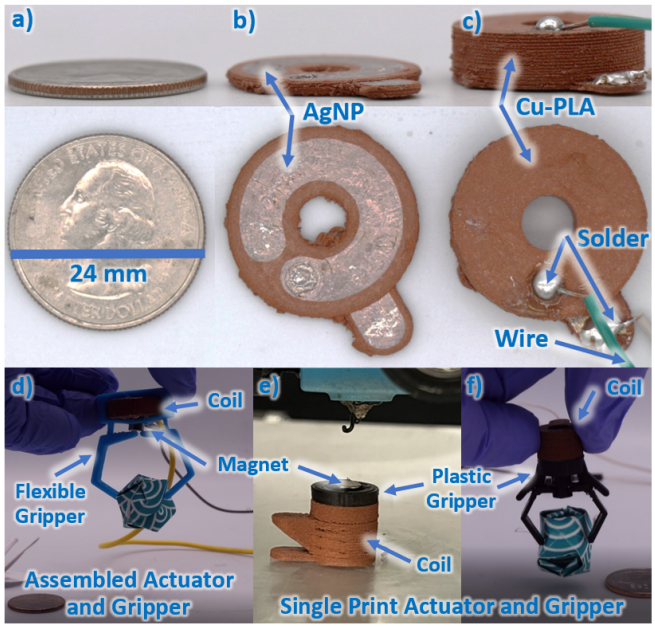

Fig. 1. A 16 layer coil is 3D printed with conductive silver nano-particles (AgNP) embedded within an electrically insulating copper-PLA (Cu-PLA) substrate. The side and top views are shown for a) a reference coin, b) a 2-layer coil, c) and 16-layer coil. d) This can be combined with separate flexure-based gripper or e) fully-integrated into a co-fabricated single-print rigid gripper for f) grasping arbitrary objects.

*Corresponding author
[1]S. Mettes, J. Bates, and Y. C. Mazumdar are with the School of Mechanical Engineering, Georgia Institute of Technology, Atlanta, GA 30332, USA, smettes3@gatech.edu
[2]K. W. Allen is with the Georgia Tech Research Institute, Atlanta, GA 30332, USA.

more useful for robotic and mechatronic applications, significant performance improvements are needed.

In this paper, we present a novel high power (up to 90 W burst) and high operating temperature ($>140°C$) additive manufacturing concept for creating electromagnetic actuators using conductive AgNP ink and metal-filled polylactic acid (PLA). If left unsintered, copper-filled PLA (Cu-PLA) is not only electrically insulating but also has a significantly higher deflection temperature, higher heat capacity, and higher thermal conductivity than traditional filament materials. Additionally, Cu-PLA exhibits improved 3D printing characteristics and does not warp during or after printing. Using these unique materials and new coil designs, $>2\times$ higher force output with 80% lower power consumption was achieved when compared to previous work using traditional 3D-printable materials. Additionally, the maximum operating temperature was increased to $>140°$C, which helped enable longer operating times and higher operating power levels. Here, the manufacturing process, material selection, and the coil design, as shown in Fig. 1, are first described. Then, the thermal, force, and dynamic mechanical responses are modeled and characterized. Finally, a compliant joint gripper, a fully-integrated single-print actuator and gripper, and a speaker application are demonstrated to show the capabilities of this high temperature, fully 3D printed actuator.

II. MATERIALS AND MANUFACTURING

Developing a fully 3D printed, multi-material, and high operating temperature electromagnetic coil for actuator applications requires the exploration of several new materials and techniques. Here, we discuss material selection of electrical and thermal properties, the design of a custom multi-material printer, and novel procedures for planning the layout of continuous multi-layer coils.

A. Material Selection for 3D Printing

High power electromagnetic coils require a combination of electrically conductive and electrically insulating materials. Additionally, since high power actuators are typically limited by their operating temperature, both materials also need to maintain their dimensions at high temperatures, have high thermal conductivities to dissipate heat, and high heat capacitances to extend transient run times. Several additively manufacturable conductive materials like solders, metal paints, and conductive filaments were considered. Ultimately silver nanoparticle ink (SmartInk S-CS21303) was selected as the main conductor due to its high post-sintering electrical conductivity, high operating temperature, and compatibility with additive manufacturing methods.

In order to select electrically insulating materials, several polymers were considered including ColorFabb nGen, PLA, polycarbonate, and metal-filled PLA. The printing properties and thermal properties for these materials are listed in Table I and Table II. From these tables, it is clear that the material with the highest deflection temperatures is copper-filled PLA (Virtual Foundry), which is 90% mass copper [22]. Although this material is designed to be sintered at high temperatures (1052°C) to create solid-copper objects, when initially printed this material is electrically insulating. Without sintering, the material has $1.8\times$ the volumetric heat capacity of nGen and $10\times$ the thermal conductivity. These properties allow heat to be more uniformly distributed and removed from the actuator surface as well as enable longer and higher power operation before melting, deformation, or other modes of failure. Thus, this unique material, that was not designed to be used as a thermally conductive electrical insulator, was selected to enable 3D printing of novel high-power and high-temperature electromagnetic coils.

TABLE I
DEFLECTION AND PRINT TEMPERATURES

Material	Deflection Temp. at 0.455 MPa	Print Temp.
nGen [18]	71 $°C$	220 $°C$
PLA [20]	49 $°C$	170 $°C$
Polycarbonate [21]	140 $°C$	290 $°C$
Cu-PLA [22]	$>140°C$	220 $°C$

TABLE II
SUBSTRATE THERMAL PROPERTIES

Material	Thermal Conductivity (W/mK)	Specific Heat (J/gK)	Density (g/cm^3)
nGen [18]	0.032 to 0.170[a]	1.1[a]	1.2
PLA [23][24]	0.032 to 0.170	1.80	1.24
Polycarb. [25]	0.173 to 0.210	1.70	1.26
Cu-PLA [22][26]	2.50 to 2.60	0.48[a]	5.00

[a] Measured or estimated in this work

B. Multi-Material Printer

To additively manufacture a two material high-power coil, both fused filament fabrication and high precision syringe deposition tools were combined on a modified FFF printer base (Creality CR-10 S4). Here, FFF is implemented across two extruders to print electrically insulating materials as well as a wide range of other filament material options. For Cu-PLA printing, a 0.6 mm stainless steel nozzle was used [26]. For AgNP deposition, a custom syringe pump system with

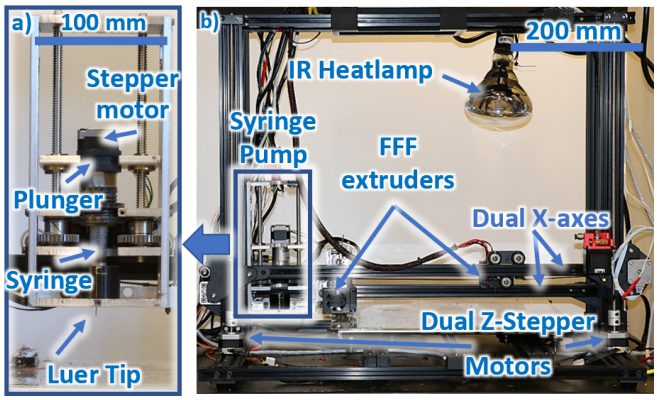

Fig. 2. Custom multi-material 3D printer is shown. a) The custom syringe pump system for printing AgNP ink includes stepper motors, gears, plungers, and a syringe. b) The full system also includes FFF extruders, dual X-axes, and an IR heatlamp for curing AgNP ink.

stepper motors was designed in order to enable rapid extrusion with moderately high precision. With a blunt tip Luer 22 gauge needle for extrusion a repeatability of <0.2 mm in the X and Y directions was achieved for the depositon of low resistance electrical traces. As shown in Fig. 2, both the FFF and syringe toolheads were mounted on independent X-axis rails, which are each operated independently in the Z-direction via dual Z-stepper motors. Independent X and Z operation of each toolhead maximizes AgNP lifespan by moving the ink away from the hot bed and curing lamp while idle. After depositing each layer, AgNP ink was sintered for 15 minutes with a 125 W infrared heat lamp, which along with the heated bed enabled the system to quickly achieve the target sintering temperature of 80°C [27].

C. Electromagnetic Actuator Design and Manufacturing

To develop an efficient and compact linear electromagnetic solenoid actuator, a 6.35 mm diameter × 6.35 mm tall cylindrical N52 neodymium iron boron (Nd-Fe-B) permanent magnet was chosen as the magnetic field source. Based on these dimensions, an electrical trace with a 5 mm inner radius and 10 mm outer radius was selected. In order to improve structural integrity, promote layer adhesion, and prevent delamination, 1.5 mm of insulation material was added to each side of the conductor. This led to coil dimensions of 3.5 mm for the inner radius, 11.5 mm for the outer radius, and 0.325 mm magnet-to-coil gap.

A total of 16 planar vertically stacked coils, each spaced 0.4 mm apart in the Z-direction, were printed in order to achieve a total coil length equal to the height of the magnet. Here, each planar coil completes 310 degrees of rotation, terminating at a 4 mm diameter and 0.4 mm tall channel composed of four 0.1 mm substrate layers. This channel, which is centered at a distance of 7.5 mm from the middle of the coil, is filled with AgNP and serves as an electrical via between layers to create a continuous counter-clockwise coil. In this work, the Z-separation of each AgNP layer was carefully selected to ensure that the nanoparticle ink was deposited on fully flat and smooth surfaces (achieved using an ironing step [28]) while also minimizing the distance between planar coils.

Figure. 3 shows the full manufacturing procedure for each conductive layer. In the first step, a layer of electrically insulating Cu-PLA is deposited. Then, AgNP is added at a height of 0.1 mm above the insulating material and sintered for 15 minutes using the heat lamp. During the sintering process, glycol is evaporated and the resulting sintered AgNP reduces to a thickness between 0.01 to 0.02 mm. Next a 70% flow rate 100% fill layer of Cu-PLA is extruded at the same 0.1 mm height to create a new base substrate layer. The next (2nd) Cu-PLA layer, printed at Z = 0.2 mm is a 60% circular infill layer that fills in any gaps and accommodates for any over-extrusion from the previous layer. The 3rd and 4th Cu-PLA layers are 100% fill layers which conclude with the final ironed surface. This process is repeated until a full coil stack is created. Overall, this printing procedure was optimized for creating a flat and smooth Cu-PLA layer prior to AgNP deposition. This prevented gaps in the conductive path and ensured manufacturing reliability. While it is possible to decrease the thickness of the insulation layers, this can result in decreased layer smoothness and lower coil performance.

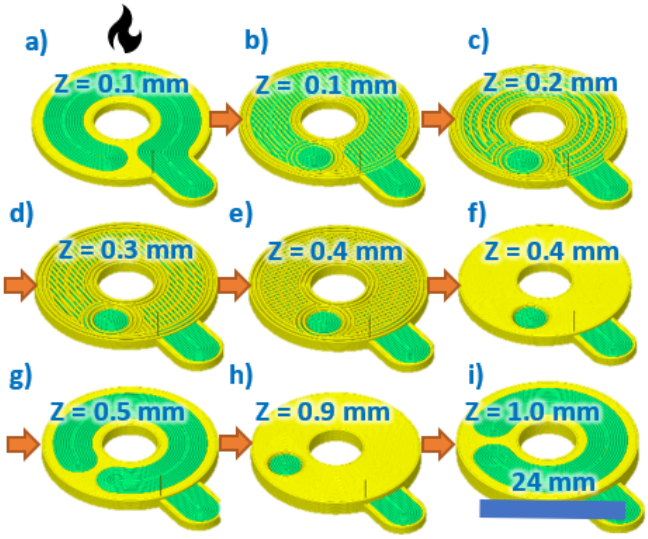

Fig. 3. The multi-material manufacturing process is shown. a) After Cu-PLA substrate deposition, the conductive AgNP is printed at Z = 0.1 mm above the base of Cu-PLA and sintered for 15 minutes, reducing the AgNP height from 0.1 to <0.01 mm. b) Then, a 70% flow rate, 100% fill Cu-PLA layer is placed on top the AgNP at a height of 0.1 mm. c) A 60% Cu-PLA infill layer is placed at Z = 0.2. d), e) This is followed by two 100% Cu-PLA infill layers (Z = 0.3 & 0.4) and f) a smoothing or ironing operation (Z = 0.4). g), h), i) Afterwards, the process is repeated and each layer is rotated clockwise by 30 degrees to enable connection vias between layers to creating a continuous 16 layer counter-clockwise coil.

III. FORCE AND THERMAL MODELS

In order to predict the behavior of the actuator and estimate the performance of different designs, models were created for the electromagnetic force output and the thermal behavior. These model predictions are later compared against experimental results.

A. Electromagnetic Force Model

In order to model the output force and electromagnetic field near the coil, the filament method [29], [30], [31] is used to calculate the axial force between the Nd-Fe-B magnet (with a surface field strength of 4000 to 5800 G) and the 1 radial layer × 16 vertical layer cylindrical coil. Here, the magnet is modeled as an equivalent current carrying wire. Using this model, the axial force between the magnet and coil is,

$$F_f(r_1, r_2, z) = \mu_0 I_1 I_2 y \sqrt{\frac{m}{4r_1 r_2}} \left(K(m) - \frac{m/2-1}{m-1} E(m)\right). \quad (1)$$

The current in the coil is expressed as I_1 and the equivalent magnet current is then $I_2 = B_r l_m/(N_m \mu_0)$. The other parameters include the permeability of free space μ_0, the center-to-center distance between the coil and magnet in the axial direction z, the permanent magnet field strength B_r, the magnet length l_m, and the equivalent number of turns in

the magnet N_m. The Legendre elliptic integrals [32], $K(m)$ and $E(m)$, are defined as,

$$K(m) = \int_0^{\pi/2} \frac{1}{\sqrt{1 - m^2 sin^2\theta}}\, d\theta, \tag{2}$$

$$E(m) = \int_0^{\pi/2} \sqrt{1 - m^2 sin^2\theta}\, d\theta, \tag{3}$$

$$m = \frac{4r_1 r_2}{(r_1 + r_2)^2 + z^2}. \tag{4}$$

The axial force between the coils and the magnet can then be calculated using superposition,

$$F_m(Y_m) = \sum_{n_m=1}^{N_m} \sum_{n_r=1}^{N_r} \sum_{n_z=1}^{N_z} F_f\left(r(n_r), R_m, z + L(n_m, n_z)\right), \tag{5}$$

$$r(n_r) = R_c + \frac{n_r - 1}{N_r - 1}\left(R_c - r_c\right), \tag{6}$$

$$L(n_m, n_z) = -\frac{1}{2}(l_m + l_c) + \frac{n_z - 1}{N_z - 1} l_c + \frac{n_m - 1}{N_m - 1} l_m. \tag{7}$$

Here, N_r is the number of radial loops, N_z is the number of axial coil layers, R_c is the outer trace radius, r_c is the inner trace radius, and l_c is the total coil height. Because current takes the shortest path through a coil and there is only one coil per layer, Eqn.(6) is simplified to $r(n_r) = r_c$ for the design described in this paper. This filament method model successfully captures the majority of the physical effects needed to estimate the force output.

B. Thermal Modeling

In order to approximate the thermal behavior of the additively manufactured coil at different input power levels, a simplified time-dependent temperature model is created. Although electrically insulating materials typically have relatively low thermal conductivities, the Cu-PLA material used in this work has a thermal conductivity that is 10× higher than most other 3D printable substrate materials. This leads to a low Biot number $Bi = hV/(kA_c)$ of 0.05 for this coil geometry. Here, the characteristic length is determined by the ratio of the body volume V to the surface area A_c, the heat transfer coefficient h, and the conductivity of substrate k. Since the Biot number is significantly less than unity, a lumped capacitance model can be used following the linear ordinary differential equation [33],

$$q_{in} = mc_p \frac{dT(t)}{dt} + hA\left(T(t) - T_0\right), \tag{8}$$

where q_{in} is the input power to the coil, c_p is the specific heat of the substrate, m is the mass of the substrate, T_0 is the ambient air temperature, A is the surface area of the coil, and $T(t)$ is the temperature of the substrate as a function of time. The solution to this equation is,

$$T(t) - T_0 = \frac{q_{in}}{hA}\left(1 - e^{-\frac{hA}{mc_p}t}\right) + \left(T(0) - T_0\right) e^{-\frac{hA}{mc_p}t}, \tag{9}$$

where T(0) is the starting temperature of the coil. Using this heat transfer model, the operating temperature as a function of time can be estimated and the maximum operating power can be determined.

IV. EXPERIMENTAL RESULTS

A. Output Force Characterization

In order to use the additively manufactured actuators for mechatronic and robotic applications, the force output of the actuators must be well understood. Here, the actuator performance at different input power levels is measured using a force sensor. A comparison of the 1 radial × 16 vertical Cu-PLA coils and the 3 radial × 12 vertical nGen substrate electromagnetic solenoids developed in our previous work [19] are illustrated in Fig. 4. It should be noted that because there are fewer total windings, the Cu-PLA solenoid has a resistance of 1 Ω compared to the resistance of 4.5 Ω for the nGen coil. Nevertheless, the force output per amp of the Cu-PLA coil is 44% higher (both the 4.1 W, 3 × 12 nGen coil and the 0.8 W, 1 × 16 Cu-PLA coils operated at at 0.9 A). The force per unit of input power also increased by 294% from 3.9 mN/W for the nGen coil to 11.46 mN/W for the Cu-PLA. This effect is mostly due to a more efficient coil design, which reduced the number of radial loops and put the conductive traces closer to the permanent magnet.

The theoretical models for each test condition were also generated and are displayed as dotted lines in Fig. 4). Here, Cu-PLA substrate coil is modeled with a single 5.5 mm inner radius winding per layer to account for minimum distance between the inner edge of the via to the center of the actuator. The nGen substrate coil is modeled with 3 evenly spaced coils per layer with a 4.5 mm inner diameter and an 18 mm outer diameter. To accurately capture the properties of the permanent magnet, the surface field was measured using a gaussmeter and mapped back to a magnetic field strength of 4000 G. Overall, the theoretical model for these additively manufactured actuators matches well with the experimental results, illustrating how performance can be accurately predicted during design.

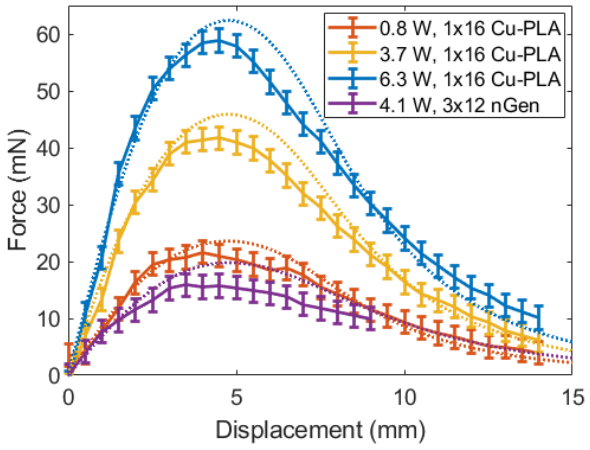

Fig. 4. The force output of the Cu-PLA substrate solenoid (1 radial × 16 vertical layers, 5 mm inner diameter, 10 mm outer diameter) with different input power levels is compared to prior work [19] with an nGen substrate solenoid (3 radial × 12 vertical layers, 4.5 mm inner diameter, 18 mm outer diameter). Solid lines indicate experimental data and dotted lines indicate the theoretical force output based on the filament method.

B. Thermal Performance

Improving the thermal performance of the actuator is critical for achieving high force output. For these experiments, a separate 1 × 16 nGen coil with the same dimensions as the Cu-PLA coil was manufactured for comparison. The thermal performance of the 1 × 16 Cu-PLA and 1 × 16 nGen coils were assessed at three different input power levels (2 W, 3.2 W, and 4.2 W) without external cooling. The temperature of each coil was measured with a platinum resistor temperature detector (Omega F2020-1000-B-100), mounted on the top surface. All tests started with the coil at ∼30 °C and DC power was applied until steady state or the maximum temperature thresholds (110°C for nGen and 160°C for Cu-PLA) were reached.

In all the cases shown in Figs. 5 and 6, the experimental data were compared with the theoretical heat transfer model. The heat transfer coefficient h in each case included natural convection and radiation effects on the top and side surfaces, and conduction through the bottom of the actuator to a metal plate through a small air gap. Based on this model, the h values ranged from 21 to 28 W/mK due to changes in radiative heat transfer and properties as a function of temperature. The remaining differences between the model and experimental results could be due to imperfections in the 3D printed object, resulting in internal air pockets, variations in contact resistance due to surface roughness, and uncertainties in thermal properties. Nevertheless, the model and experimental data matched well, indicating that thermal performance can be estimated accurately during design.

Temperature measurements for the nGen substrate coil are described in Fig. 5. Here, the temperature reaches steady state while remaining below the threshold temperature only for the case with 2.0 W of input power. The thermal time constant was determined to be 147 s. Above an input power of 2 W, the temperatures increased above 110°C within 3 minutes. Sustaining higher temperatures with the nGen substrate leads to coil failure via delamination between the AgNP and nGen layers, resulting in breaking of the trace.

The Cu-PLA substrate, on the other hand, has an ∼80%

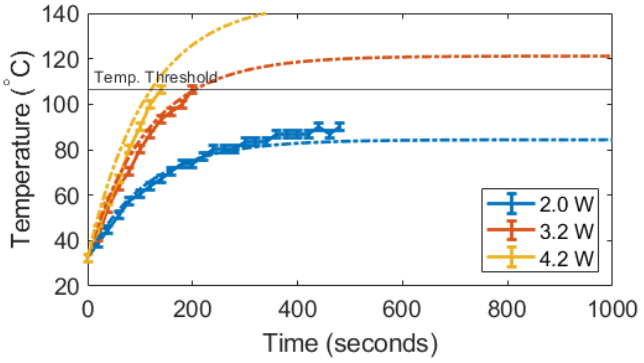

Fig. 5. The temperature of a nGen substrate coil stabilized at 90°C at an input power of 2.0 W. The time constant was observe to be 147 seconds. Solid lines indicate experimental data and dotted lines indicate the theoretical heat transfer model. Beyond 110°C the nGen coil deformed, causing delamination and AgNP trace breakage.

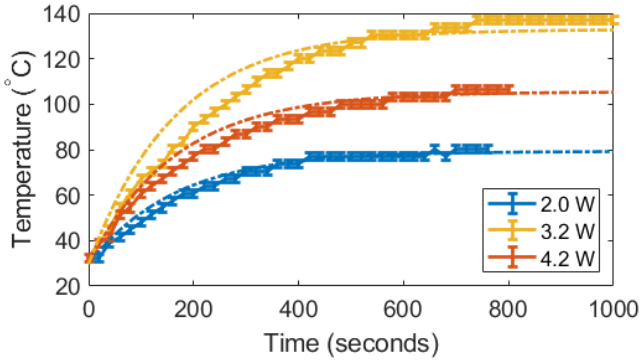

Fig. 6. The temperature of the Cu-PLA substrate coils stabilized at 80°C, 110°C, and 140°C for input power levels of 2.0 W, 3.2 W, and 4.2 W, respectively. The thermal time constant was observed to be 222 seconds. Solid lines indicate experimental data and dotted lines indicate the theoretical heat transfer model. Peak operating temperatures as high as 190°C were achieved for the Cu-PLA substrate prior to deformation, delamination, and AgNP trace breakage.

higher volumetric heat capacity due to its 417% higher density (see Table II) than the nGen material. As a result, the Cu-PLA coil showed significantly improved performance over the nGen coil, as illustrated in Fig. 6. Here, the time constant for reaching the steady state temperatures (80°C, 110°C, and 140°C for 2 W, 3.2 W, and 4.2 W, respectively) was estimated to be 222 s, which is 150% longer than the nGen coil. A longer time constant enables the coil to be operated at high power levels for longer periods of time, thus extending the force output and application space for this actuator. Additionally, the Cu-PLA coils are able to operate up to 4.2 W without reaching their maximum operating temperature, which is above 140°C. In some cases, the Cu-PLA coils were operated at up to 90 W and 190°C for short intermittent periods without damage.

The most common failure mode for Cu-PLA coils is entirely different from nGen coils. The low temperature

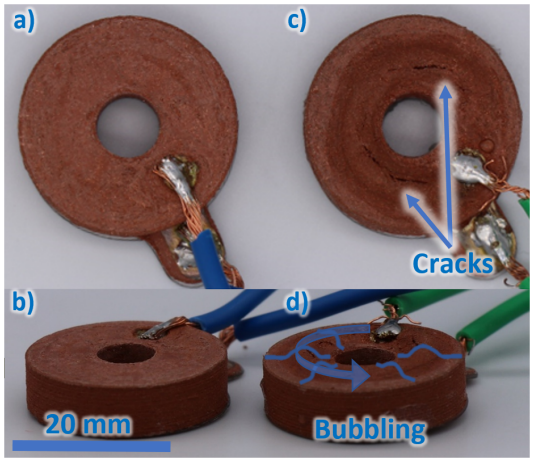

Fig. 7. The primary failure mode of the Cu-PLA solenoid is cracking caused by rapid boiling of remaining glycol from the AgNP ink. a) The top and b) side views of a functional solenoid are shown for comparison. c) The top and d) side of a failed solenoid show deformations and cracks in the top surface from glycol boiling, resulting in a broken coil circuit. Failures occurred under high peak input power tested at up to 90 W.

sintering process for AgNP ink (below 100°C) implemented in the manufacturing process described in this work does not entirely boil off the glycol solution in the nanoparticle ink. As the solenoid temperature rises above 160°C for sustained periods, the glycol boils and deforms the solenoid directly above the AgNP traces. At these temperatures further sintering of the nanoparticles can occur which reduces overall coil resistivity. However, this also causes cracks and bubbling as shown in Fig. 7. Additional improvements in the manufacturing process can potentially help eliminate this high temperature failure mode. Overall, these results illustrate vastly improved performance for Cu-PLA coils.

C. Dynamic Mechanical Response

Understanding the bandwidth and dynamic response of the actuator is critical for high speed actuation and precision control applications. Here, the combined performance of the Cu-PLA coil, Nd-Fe-B magnet, and an external spring is shown in Fig. 8. To acquire the frequency data, the solenoid is actuated using a high power motor driver (Pololu G2 18v25) reproducing a square wave input from a signal generator. Several 6-second chirps in the ranges of 1 to 250 Hz, 250 to 500 Hz, 500 to 1000 Hz, 1.0 to 1.5 kHz, and 1.5 to 20 kHz were used. Input power to the solenoid was fixed at 16 W and external cooling from a 12 V 100 mm diameter fan was used. To capture the displacement data, the magnet position was tracked at high magnification with a Phantom VEO-E 310L color high-speed camera at 40 kHz. After data collection, the position of the magnet was tracked using a custom machine vision centroid detection algorithm.

Next, to process the frequency response, transfer function estimation and windowing techniques [34] were applied to the 5 datasets and the aggregated results are shown in Fig. 8. The magnitude-squared coherence (MSC) indicate the portion of the response that can be modeled using linear elements. The grayed region in each plot indicates frequencies where the response was small (sub-pixel) and the uncertainties are large. Based on the experimental results and phase plots, a resonance frequency of 25 Hz and a bandwidth of 28 Hz was determined for this actuator.

If a mass-spring-damper model is used, a transfer function of $X_o(s)/F(s) = G/\left(M_m s^2 + bs + k\right)$ can be derived. Here, $F(s)$ is the input force, X_o the magnet displacement, and G the transfer function gain. The constants M_m, b, and k, are the mass, damping, and spring constants of the system. The mass of the magnet was measured to be 2.75 g, the spring constant was calculated to be 165 N/m, and the damping ratio was determined to be $\zeta = 1/2 \cdot b/M_m \cdot \sqrt{k/M_m} = 0.05$ based on the model. Overall, the model and measured responses match well except for the 122 Hz resonance, which is likely caused by a structural resonance from mounting components.

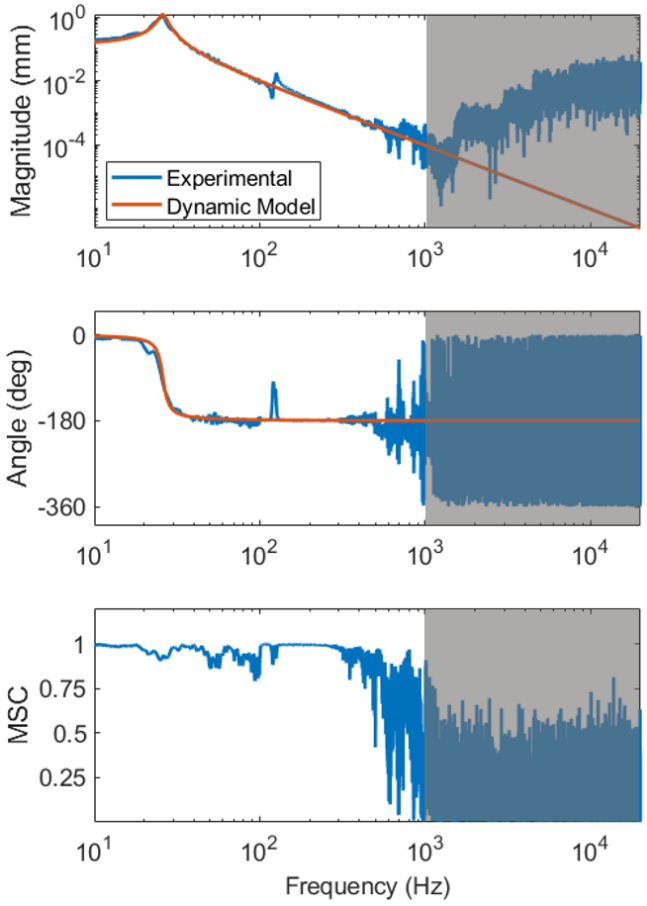

Fig. 8. The dynamic mechanical response of the fully 3D printed solenoid with an additional spring is shown. The magnitude (top), phase (middle) and magnitude-squared coherence (MSC) (bottom) were determined using high-magnification, high-speed camera tracking a chirped input. The gray area indicates frequencies with sub-pixel motion and high uncertainty.

V. APPLICATIONS

A. Compliant Joint Gripper

The increased output power and operating temperature of the additively manufactured Cu-PLA coils enables several different applications. Figure 9 shows how the fully 3D

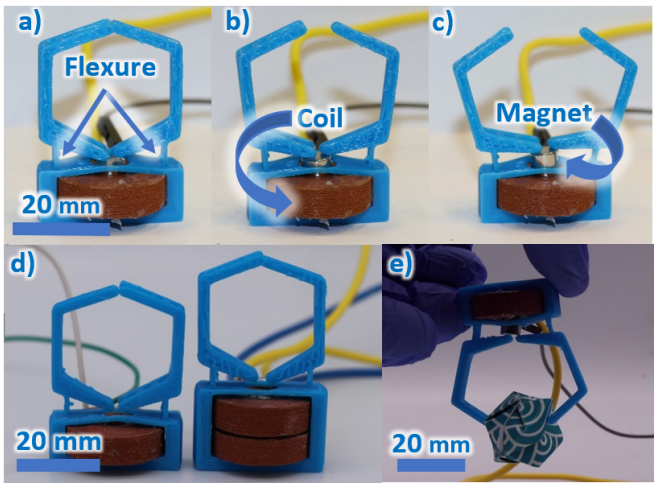

Fig. 9. A robotic gripper application is shown where the 3D printed coil is coupled with a Nd-Fe-B magnet and 3D printed flexure. The gripper is shown in a) closed, b) partially open, and c) fully open states. d) The actuator is modular and can be stacked to increase stroke. e) A gripping example is also illustrated.

printed coil can be combined with a Nd-Fe-B magnet and a soft 3D printed flexure structure to create a functional force-controlled robotic compliant joint gripper. The gripper opens when power is applied (with a maximum opening space of 15 mm) and returns to a closed state when power is reduced. With this Cu-PLA solenoid, the gripper can provide up to 50 mN of continuous force for opening or closing. For short bursts (∼3 seconds) up to 150 mN (60 W of input power) of opening or closing force can be generated. Figure 9 illustrates how the gripper can be used to pick up an origami cube and the supplementary video shows how the force-driven gripper can be used to grasp several other objects of different shapes. Because the design is modular, it is also possible to double the stroke of the actuator by simply stacking two solenoids.

B. Audio Speaker

The high power and high operating temperature Cu-PLA coil can also be used to drive a 3D printed speaker, as illustrated in Fig. 10. Here, the Cu-PLA coil and Nd-Fe-B magnet are used to drive a 60 mm diameter speaker cone. While operating with 8 W of power, the speaker is able to produce up to 82 dB in audio output power at 3 kHz measured from a distance 20 cm from the cone. For these measurements, the ambient noise ranged from 30 to 50 dB. The speaker system is able to produce sound across the entire audio range, but is most effective while operating below 10 kHz. The supplementary video included with this paper illustrates how this actuator can be used to play simple tunes.

C. Fully Integrated 3D Printed Gripper

One of the most important benefits of a fully 3D printed actuator is the ability to manufacture actuators directly into a 3D printed mechanism. In this work, we demonstrate a multi-material, single print actuator and miniature gripper, as shown in Fig. 11. Here, the actuator is constructed

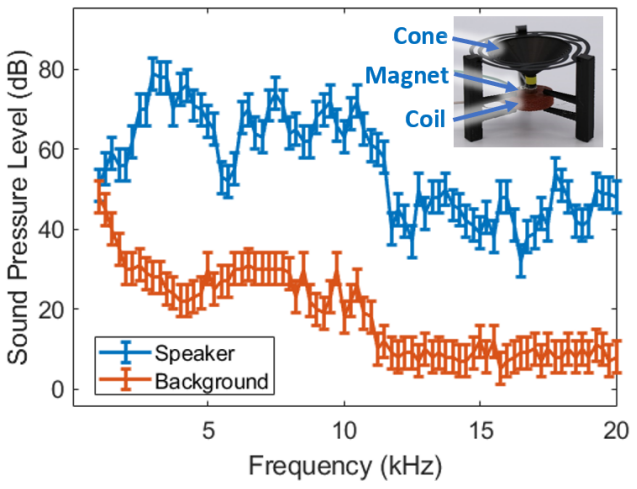

Fig. 10. The fully 3D printed coil can be used as a speaker when combined with a magnet, cone, and spring. The speaker output at multiple frequencies between 0 and 20 kHz is shown. For an input power of 8 W, the maximum audio output was measured to be 82 dB at a distance of 20 cm away from the speaker cone. This was measured against a background of 30 dB.

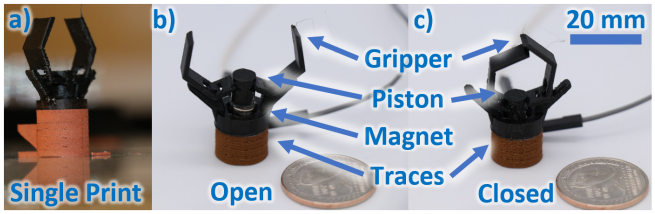

Fig. 11. A fully 3D printed actuator and gripper can be co-fabricated within a single 3D print. This demonstration shows how coils can be fully integrated in the multi-material additively manufactured components. The gripper is shown a) post printing and in b) open and c) closed states.

from Cu-PLA and AgNP and the gripper mechanism is constructed from PLA (note that the custom printer has 2 FFF extruders and one syringe pump for nanoparticles). The only component that is not printed is the permanent magnet, which can be inserted mid-print (using manual or pick and place processes) or added after printing is complete. The gripper design in this case uses a piston design which pushes or pulls on two gripper arms that connected to the body using revolute joints. The gripper opens and closes by up to 27 mm and can be controlled by applying positive or negative voltage to the 3D printed coil. The supplementary video shows the operation of this coil mechanism for grasping arbitrarily-shaped objects. Overall, this demonstration shows how 3D printed electromagnetic actuators can be directly integrated into mechanism designs and manufactured in a single print.

VI. CONCLUSION

In this paper, we describe a novel 3D printed electromagnetic coil that is created using silver nanoparticles for electrical traces and copper-filled plastics for electrical insulation. This combination of materials allows the coil to operate at significantly higher input power levels and steady state temperatures (>140°C) than for the case where more traditional plastics are used. The combination of an improved coil design and the use of unique materials increased the force output by 294% over previous work, extended the time constant by over 150% over plastic materials, and raised the operating temperature by 50 to 80°C over traditional electrically insulating filaments. The actuator described in this work is capable of operating with up to 60 W of input power for short periods (<3 seconds) with an output force of up to 150 mN. Conversely, for steady state applications, this actuator can operate continuously at up to 4.2 W with an output of 60 mN. Using this new actuator, several applications were demonstrated including a speaker and a gripper application. Uniquely, we also demonstrate co-fabrication of the 3D printed electromagnetic actuator with a gripper in a single 3D print, showing how more complex active components can be integrated.

When the Cu-PLA actuator (volume of 3743 mm^3) is compared with a commercial Transmotec F0520L solenoid (volume of 4160 mm^3) of a similar size [35], it is clear that the current Cu-PLA design is less efficient. The Cu-PLA actuator operates at ∼10% of the peak force and

58% of the continuous force while requiring ∼260 to 750% more power. Although the 3D printed solenoid does not provide an equivalent output force for the same volume, the ability to directly integrate the actuator within a 3D printed mechanism, the customizability of the actuator design, and the ease of prototype iteration make this actuator design concept extremely useful.

Several areas could potentially be improved in the future to further extend the capabilities of the fully 3D printed high operating temperature electromagnetic actuator. The resistivity of the electrical traces, for example, can be improve by altering dimensions and increasing AgNP curing temperature. The packing density can also be increased by reducing the thickness of the electrically insulating layers via more advance deposition, ironing, and smoothing methods. Overall, with the ability to use multi-material printing techniques, it is now possible to create actuators within 3D printed parts and produce more complex, active components. This could help reduce manufacturing costs, improve customization, and reduce prototyping/design time for future mechatronic and robotic systems.

ACKNOWLEDGMENTS

The authors would like to thank the Georgia Tech Research Institute (GTRI) Graduate Student Fellowship Program for their support and the Dynamic Adaptive Robotic Technologies (DART) laboratory for assistance with equipment.

REFERENCES

[1] E. Aguilera, J. Ramos, D. Espalin, F. Cedillos, D. Muse, R. Wicker, and E. MacDonald, "3D printing of electro mechanical systems," in *2013 International Solid Freeform Fabrication Symposium*, 2013.

[2] D. S. Vorunichev, "Application of additive technology for 3D printing of electronic devices as a way to reduce prototyping time," in *2021 International Conference on Quality Management, Transport and Information Security, Information Technologies (ITQMIS)*, 2021, pp. 480–483.

[3] B. Lu, H. Lan, and H. Liu, "Additive manufacturing frontier: 3D printing electronics," *Opto-Electron Adv*, vol. 1, no. 1, pp. 170 004–170 004, 2018.

[4] B. B. Narakathu, A. Eshkeiti, A. S. G. Reddy, M. Rebros, E. Rebrosova, M. K. Joyce, B. J. Bazuin, and M. Z. Atashbar, "A novel fully printed and flexible capacitive pressure sensor," in *IEEE Sensors*, 2012, pp. 1–4.

[5] J. Courbat, Y. Kim, D. Briand, and N. de Rooij, "Inkjet printing on paper for the realization of humidity and temperature sensors," in *2011 16th International Solid-State Sensors, Actuators and Microsystems Conference*, 2011, pp. 1356–1359.

[6] S. Agarwala, G. L. Goh, Y. L. Yap, G. D. Goh, H. Yu, W. Y. Yeong, and T. Tran, "Development of bendable strain sensor with embedded microchannels using 3D printing," *Sensors and Actuators A: Physical*, vol. 263, pp. 593–599, 2017.

[7] Y. Gu, D. Park, D. Bowen, S. Das, and D. R. Hines, "Direct-write printed, solid-core solenoid inductors with commercially relevant inductances," *Advanced Materials Technologies*, vol. 4, no. 1, p. 1800312, 2019.

[8] P. Lall, J. Narangaparambil, V. Soni, and S. Miller, "Sintering process conditions for additive printing of multi-layer circuitry aerosol-jet process in conjunction with nanoparticle ink," in *2020 19th IEEE Intersociety Conference on Thermal and Thermomechanical Phenomena in Electronic Systems (ITherm)*, 2020, pp. 805–813.

[9] S. B. Fuller, E. J. Wilhelm, and J. M. Jacobson, "Ink-jet printed nanoparticle microelectromechanical systems," *Journal of Microelectromechanical Systems*, vol. 11, no. 1, pp. 54–60, 2002.

[10] H. Peng, F. Guimbretière, J. McCann, and S. Hudson, "A 3D printer for interactive electromagnetic devices," in *Proceedings of the 29th Annual Symposium on User Interface Software and Technology*. Association for Computing Machinery, 2016, p. 553–562.

[11] A. Elaskri and A. Ellery, "Developing techniques to 3D print electric motors," in *Proceedings of the International Symposium Artificial Intelligence Robotics & Automation in Space, Madrid, Spain*, 2018, pp. 4–6.

[12] Y. Yan, J. Moss, K. D. T. Ngo, Y. Mei, and G.-Q. Lu, "Additive manufacturing of toroid inductor for power electronics applications," *IEEE Transactions on Industry Applications*, vol. 53, no. 6, pp. 5709–5714, 2017.

[13] L. Li, R. Abedini-Nassab, and B. B. Yellen, "Monolithically integrated Helmholtz coils by 3-dimensional printing," *Applied Physics Letters*, vol. 104, no. 25, p. 253505, 2014.

[14] N. Lazarus, S. S. Bedair, and G. L. Smith, "Creating 3D printed magnetic devices with ferrofluids and liquid metals," *Additive Manufacturing*, vol. 26, pp. 15–21, 2019.

[15] N. Kohls, B. Dias, Y. Mensah, B. P. Ruddy, and Y. C. Mazumdar, "Compliant electromagnetic actuator architecture for soft robotics," in *2020 IEEE International Conference on Robotics and Automation*, 2020, pp. 9042–9049.

[16] N. Kohls, I. Abdeally, B. P. Ruddy, and Y. C. Mazumdar, "Design of a Xenia coral robot using a high-stroke compliant linear electromagnetic actuator," *ASME Letters in Dynamic Systems and Control*, vol. 1, no. 3, 2021.

[17] R. Balak and Y. C. Mazumdar, "Bistable valves for MR fluid-based soft robotic actuation systems," *IEEE Robotics and Automation Letters*, vol. 6, no. 4, pp. 8285–8292, 2021.

[18] colorFabb, *Technical datasheet nGen*, 2020.

[19] S. Mettes, N. Kohls, K. W. Allen, and Y. C. Mazumdar, "Characterization of a 3D printed electric solenoid with multi-layer silver nanoparticle traces," in *2022 AACC Modeling, Estimation and Control Conference (MECC)*, 2022.

[20] SD3D, *SD3D PLA Technical Data Sheet*, 2022.

[21] MatWeb, *Deflection Temperature Testing of Plastics*, 2022.

[22] The Virtual Foundry, *Copper Filament*, 2022.

[23] MatWeb, *Overview of materials for Polylactic Acid (PLA) Biopolymer*, 2022.

[24] SD3D, *PLA Technical Data Sheet*, 2022.

[25] Matweb, *Overview of materials for Polycarbonate, Extruded*, 2022.

[26] M. Nikzad, S. H. Masood, and I. Sbarski, "Thermo-mechanical properties of a highly filled polymeric composites for fused deposition modeling," *Materials & Design*, vol. 32, no. 6, pp. 3448–3456, 2011.

[27] Sigma-Aldrich, *Technical datasheet for Ag nanoparticles ink, Part Number 901090*, 2022.

[28] J. O'Connel, "Cura: Ironing - simply explained," Oct. 2021. [Online]. Available: https://all3dp.com/2/cura-ironing-3d-printing-ironing/

[29] W. Robertson, B. Cazzolato, and A. Zander, "Axial force between a thick coil and a cylindrical permanent magnet: Optimizing the geometry of an electromagnetic actuator," *IEEE Transactions on Magnetics*, vol. 48, no. 9, pp. 2479–2487, 2012.

[30] S. I. Babic and C. Akyel, "Magnetic force calculation between thin coaxial circular coils in air," *IEEE Transactions on Magnetics*, vol. 44, no. 4, pp. 445–452, 2004.

[31] A. Shiri and A. Shoulaie, "A new methodology for magnetic force calculations between planar spiral coils," *Progress in Electromagnetics Research*, vol. 95, pp. 39–57, 2009.

[32] H. Alzera and S.-L. Qiub, "Monotonicity theorems and inequalities for the complete elliptic integrals," *Journal of Computational and Applied Mathematics*, vol. 172, no. 2, pp. 289–312, 2004.

[33] F. P. Incropera, D. P. D. T. L. Bergman, and A. S. Lavine, *Fundamentals of heat and mass transfer*. Wiley New York, 1996, vol. 6.

[34] Y. Chen and I. W. Hunter, "Stochastic system identification of skin properties: Linear and Wiener static nonlinear methods," *Annals of Biomedical Engineering*, vol. 40, no. 10, pp. 2277–2291, 2012.

[35] Transmotec, "Solenoids and holding magnets." [Online]. Available: https://www.transmotec.com/product-category/solenoids/